



(This is a sample cover image for this issue. The actual cover is not yet available at this time.)

This article appeared in a journal published by Elsevier. The attached copy is furnished to the author for internal non-commercial research and education use, including for instruction at the authors institution and sharing with colleagues.

Other uses, including reproduction and distribution, or selling or licensing copies, or posting to personal, institutional or third party websites are prohibited.

In most cases authors are permitted to post their version of the article (e.g. in Word or Tex form) to their personal website or institutional repository. Authors requiring further information regarding Elsevier's archiving and manuscript policies are encouraged to visit:

<http://www.elsevier.com/copyright>

Contents lists available at [SciVerse ScienceDirect](http://www.sciencedirect.com)

## Earth and Planetary Science Letters

journal homepage: [www.elsevier.com/locate/epsl](http://www.elsevier.com/locate/epsl)

## Equatorial glaciations on Mars revealed by gravitational collapse of Valles Marineris wallslopes

Daniel Mège<sup>a,b,\*</sup>, Olivier Bourgeois<sup>a</sup><sup>a</sup> Laboratoire de planétologie et géodynamique, UMR CNRS 6112, Université de Nantes, 2 rue de la Houssinière, BP 92205, 44322 Nantes, France<sup>b</sup> Now at Institute of Geological Sciences, Polish Academy of Sciences, Research Centre in Wrocław, Podwale St. 75, 50-449 Wrocław, Poland

## ARTICLE INFO

## Article history:

Received 9 May 2011

Received in revised form 19 August 2011

Accepted 22 August 2011

Available online xxxx

Editor: T. Spohn

## Keywords:

sackung

deep-seated gravitational spreading

Valles Marineris

Mars

glaciation

trimline

moraine

normal faulting

## ABSTRACT

Martian global climate models that account for evidence of past glaciations reported in tropical to mid-latitude regions of Mars predict accumulation of water ice in Valles Marineris during past periods of high obliquity. Observational evidence for such glaciations is given here. Topographic basement ridges of tectonic origin are common in Valles Marineris, and display sackung features, an assemblage of tectonic patterns that are diagnostic of deep-seated gravitational slope deformation. This deformation is most easily explained by paraglacial ridge failure subsequent to ridge wall debuttressing and decohesion following the retreat of glaciers. This interpretation is supported by extensive bibliographic analysis of sackung triggers on Earth, by morphological evidence of subglacial erosion of the lower parts of Valles Marineris wallslopes, of periglacial erosion of their upper parts and by the presence of various types of glacial landforms on the floors of Valles Marineris troughs. The age of these equatorial glaciations is found to be older than 1.4 Gy and younger than 3.5 Gy.

© 2011 Elsevier B.V. All rights reserved.

## 1. Introduction

Over ~3.5 Gy of geologic record, the wallslopes of Valles Marineris, the giant equatorial trough system of Mars, have preserved many tectonic and geomorphologic processes that developed under a variety of morphoclimatic conditions. These are still debated and may include glacial, alpine, fluvial, submarine, and subglacial processes. Valles Marineris (Fig. 1) is a series of 4–10 km-deep interconnected troughs that covers a surface area of 650 by 2000 km in the equatorial region of Mars (Blasius et al., 1977; Sharp, 1973). This is basically a system of alternating, E–W striking, grabens and horsts (Mège and Masson, 1996a; Peulvast et al., 2001; Schultz, 1991, 1995) associated with large-scale collapse depressions (Schultz, 1998) that recorded a complex history of tectonic, erosional, and depositional processes (Chojnacki and Hynek, 2008; Fueten et al., 2008; Le Deit et al., 2008; Lucchitta, 1977, 1981, 1999; Lucchitta et al., 1992; Mège and Masson, 1996a; Nedell, 1987; Okubo, 2010; Okubo et al., 2008; Peulvast and Masson, 1993a,b; Peulvast et al., 2001). The horst topographic ridges display two remarkable deformation features: crestal grabens, indicating ridge-top splitting, and uphill-facing normal faults scarps on ridge flanks (Fig. 2a to f). These two features are suggestive of sackung, a

large-scale and slow mass-wasting mechanism of topographic ridges observed in formerly glaciated terrestrial mountains (e.g., Bachman et al., 2009; Hippolyte et al., 2006; Jarman, 2006; Kobayashi, 1956; Reitner and Linner, 2009; and Supplementary Table 1). Sackung (Fig. 2g–h), initially defined as a continuous, viscous mechanism of slope deformation (Zischinsky, 1966), was shown by Varnes et al. (1989) to be characterised by (1) double-crested ridges; (2) crestal grabens, symmetrical or asymmetrical; (3) uphill-facing fault scarps, striking approximately parallel with topographic contours, along the upper part of ridge slopes, and (4) bulging of the lower part of the ridge slopes; (5) ridge topography higher than 300 m.

This specific tectonic assemblage is diagnostic of gravitational spreading of topographic ridges: the development of crestal grabens (Fig. 2a–b) and uphill-facing fault scarps along ridge slopes (Fig. 2c–f) is compensated downslope by compressive bulging (Beget, 1985; Chigira, 1992; Discenza et al., 2011; Hippolyte et al., 2006, 2009; Reitner et al., 1993; Varnes et al., 1989), or thrusting of the sagging slope over the neighbouring valley (Bachman et al., 2009; Guerricchio and Melidoro, 1979; Savage and Varnes, 1987).

As we shall now discuss from examples selected in Ius Chasma, in western Coprates Chasma, at the Melas–Candor and Candor–Ophir boundaries and in Candor Chasma (Fig. 1), this specific tectonic assemblage is observed in Valles Marineris. Valles Marineris thus provides the most spectacular and comprehensive range of sackung features identified in the solar system to date.

\* Corresponding author.

E-mail addresses: [daniel.mege@twarda.pan.pl](mailto:daniel.mege@twarda.pan.pl) (D. Mège), [olivier.bourgeois@univ-nantes.fr](mailto:olivier.bourgeois@univ-nantes.fr) (O. Bourgeois).

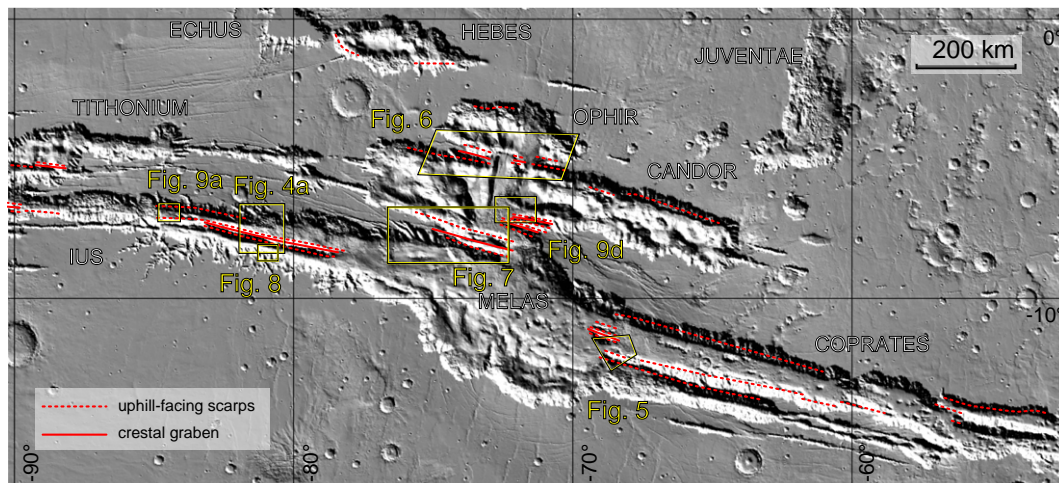


Fig. 1. Location of the main Valles Marineris chasmata, the major gravitational spreading sites, and some of the figures.

Crestal grabens and uphill-facing fault scarps have been identified using the HRSC, THEMIS, MOC, CTX image datasets, as well as topographic profiles obtained from the MOLA Precision Experiment Data Records (PEDR). Basal slope deformation has been identified and characterised using the abovementioned datasets and HiRISE images.

## 2. Sackung features in Valles Marineris

Ius Chasma displays two parallel grabens and an intervening horst, Geryon Montes, which forms a ridge showing a complex crestal graben (Figs. 2b, 3, and 4). The Geryon Montes ridge also displays ridge-parallel, up-hill facing, normal faults on its southern slope (Figs. 2c, 3 and 4). Normal faulting has not, or weakly, affected the northern ridge slope, similar to documented terrestrial sackung instances in which deformation affects one of the ridge slopes mostly, leaving the other slope almost intact (e.g., Jarman, 2006; Reitner and Linner, 2009). The stratified sedimentary material covering the basement on the floor of the graben south of Geryon Montes is folded, as was already apparent on stereoscopic Viking images (Blasius et al., 1977), in the form of a gently dipping anticline–syncline pair (Figs. 3 and 4, and Supplementary Figs. 1 and 2). Strata dip angles, as measured along MOLA PEDR profiles perpendicular to Ius Chasma, are as high as  $12^\circ$  on the fold flanks (Figs. 3 and 4).

In southwestern Coprates Chasma, sackung was locally followed by landsliding. The landslide failure plane, on the southern side of the ridge, cut through the crestal graben and the entire landslide mass moved to the north (Fig. 5). Debris apron geometry can be used to infer pristine landslide failure surface steepness; the arrow-head shape of the Coprates Chasma landslide is consistent with a deep-seated failure surface formed by reactivation of a sackung normal fault (Lucas et al., in press). At the Candor–Ophir boundary also, sackung was followed by landsliding (Lucchitta, 1999) prior to the deposition of the so-called Valles Marineris interior layered deposits (ILDs; Fig. 6). In several instances on Earth (see Supplementary Table 1), landsliding has been similarly described as a consequence of renewed slip along sackung normal faults located on the opposite ridge slope; many other terrestrial cases probably exist and await proper characterisation (Hewitt et al., 2008).

At the Melas–Candor boundary, the plateau edge, at an elevation of  $\sim 4000$  m, gradually turns into a narrow ridge that lowers and splits at the middle (Fig. 7). Ridge-top splitting and development of uphill-facing fault scarps (Fig. 2d) have proceeded until the elevation of the crestal depression decreased from ca. 4000 m to ca.  $\sim 3500$  m. A large

debris slope has developed at the eastern lateral boundary of the ridge, indicating that the ridge was much higher in the past indeed.

In addition to the selected examples described above, tectonic assemblages diagnostic of sackung are observed along the flanks of most topographic ridges in Valles Marineris (Fig. 1). In some instances (e.g., Coprates Chasma, Fig. 1), uphill-facing fault scarps are observed on the lower half of the wallslopes only. Similar basal uphill-facing normal fault scarps have been rarely described on Earth, but in areas where they were identified they were ascribed to postglacial unloading and rebound (Ustaszewski et al., 2008).

## 3. Origin of sackung features on Earth and implications for Valles Marineris

Treiman (2008) suggested that the crestal grabens of Geryon Montes may be inherited from the early rifting history of Valles Marineris (e.g., Mège and Masson, 1996a,b; Schultz, 1995) and were preserved by ridge strengthening by groundwater mineralization or dyke injection along the graben faults. Two mechanisms of ridge strengthening may be advocated, either (1) fault strengthening and fault activity locking, or (2) (Treiman, 2008) increase of erosional resistance in the graben fault zone. (1) Fault strengthening faces mechanical problems in that groundwater mineralization and other mechanisms of fault infilling are some of the fundamental processes by which stick-slip faulting is made possible (e.g., Bos and Spiers, 2002; Cowie, 1998; Marone, 1998; Olsen et al., 1998), inconsistent with strengthening of the considered volume of crust. (2) Influence of increase of erosional resistance in the graben zone on preservation of earlier graben geometry can be tested by examining ridge morphology. In case of mechanically homogeneous rock mass, spur-and-gully morphology development by erosion of an initially flat plateau is expected to produce a symmetrical ridge morphology in which the crestline separates two wallslopes of similar length. Conversely, locally increased erosional resistance along inherited plateau graben should result in development of asymmetrical ridge topography, except by coincidence, depending on the location of the inherited graben. Ius Chasma mapping (Fig. 3) reveals that Geryon Montes does not show such a topographic asymmetry. Moreover, the Candor–Ophir boundary and the Melas Chasma ridges (Figs. 6–7), which are connected to the plateau, are not aligned with nearby plateau grabens, indicating that the crestal grabens are likely not inherited from the rifting period. We infer from these considerations that the grabens inherited from Valles Marineris rifting probably



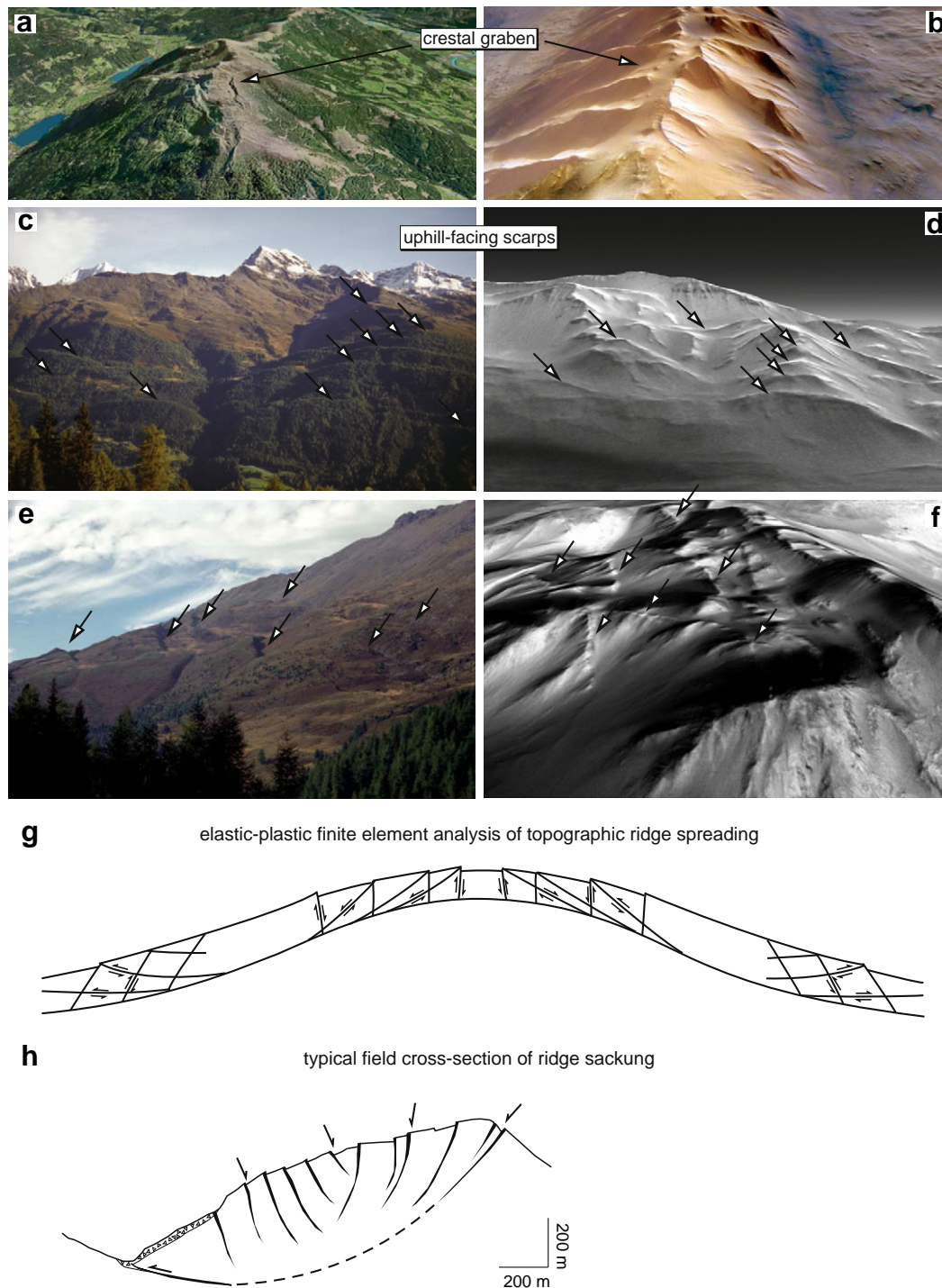


**Fig. 2.** Sackung deformation on Earth and analogue features on Mars. a, View of crestal graben at Bodeneck in the Austrian Alps. Note the glacial valleys and lakes on the ridge sides (satellite image made available by Google Earth®). b, View of crestal graben at Geryon Montes (THEMIS day IR mosaic draped over HRSC digital elevation model). North is to the right. Location in Fig. 3. c, Uphill-facing fault scarps in Tyrol, Austria, NW of Lienz (Reitner and Linner, 2009). d, Uphill-facing scarps at the Melas–Candor chasma boundary (location in Fig. 7b). North is to the background. e, Same as c, perpendicular view. f, Uphill facing fault scarps at the Candor–Ophir chasma boundary (mirrored for easier comparison with Fig. 2e). North to the left. Location in Fig. 6. g, Plastic flow of a gravitationally spreading ridge (Savage and Varnes, 1987). h, Typical geometry of sackung features from examples in crystalline and sedimentary rocks in the Tatra Mountains, modified after Mahr (1977), Nemčok (1972) and Nemčok and Baliak (1977). The thickest lines locate normal faults (on the ridge) and a thrust fault (in the valley). One of the uppermost normal faults on the ridge is connected to the basal thrust (dashed line), forming a décollement (Nemčok and Baliak, 1977). It has been suggested that a zone of crushed rocks exists instead of the décollement in crystalline basement (Mahr, 1977).

played not more than a coincidental role in the formation of the crestal grabens.

In contrast, the geometry of grabens follows the geometry of the crestline so perfectly that a major influence of body forces postdating Ius Chasma opening on their development appears likely. This

interpretation is consistent with terrestrial analogues that suggest a common origin for the specific tectonic assemblage that the crestal grabens form with uphill-facing fault scarps and basal ridge slope bulging. On Earth, this tectonic assemblage, diagnostic of sackung, has been almost exclusively observed in mountain



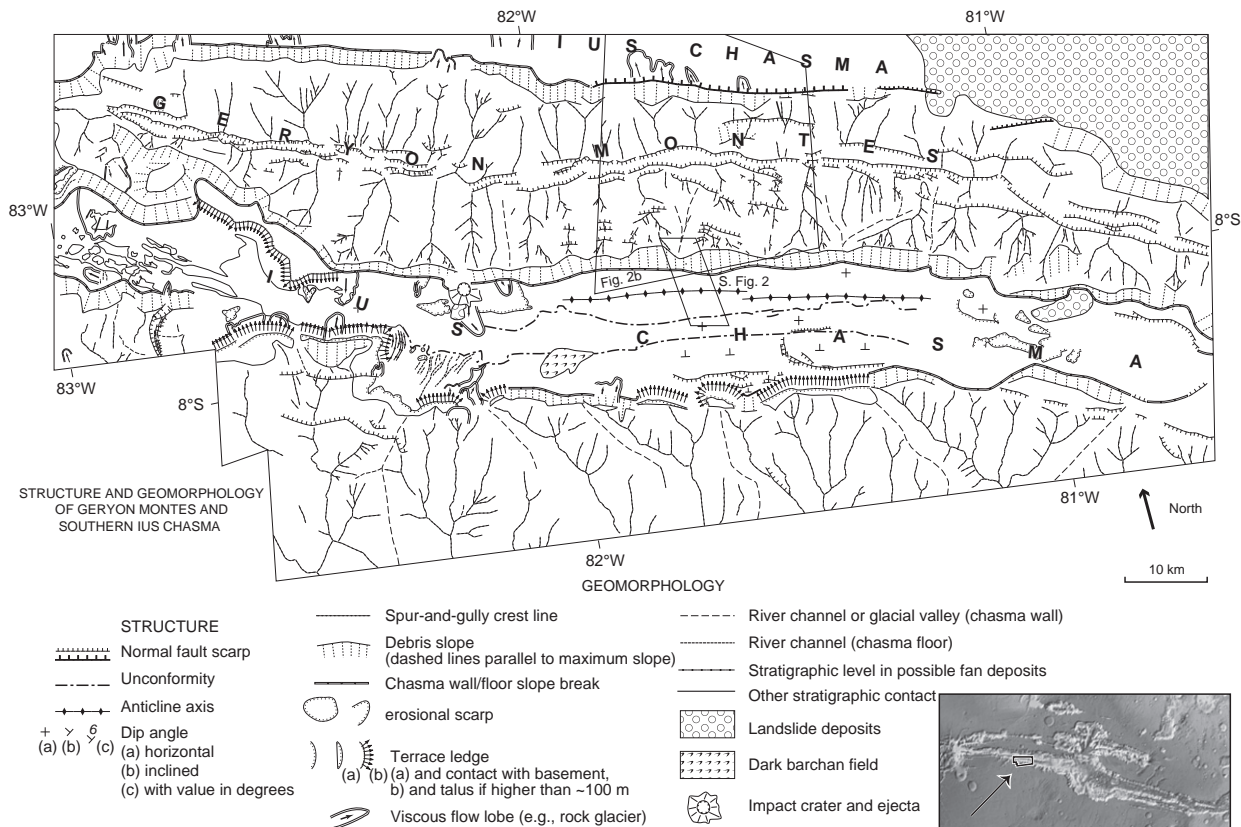


**Fig. 3.** Structural and geomorphologic map of part of Ius Chasma. Mapping has been carried out using THEMIS visible and infrared day-time and night-time images, MOC images, and CTX images. Night-time THEMIS images have been of critical help for identifying the succession of geologic units in the Ius Chasma floor.

ranges that were glaciated during the Quaternary. It has been nearly systematically attributed to paraglacial topographic readjustment. From amongst 44 articles published in peer-reviewed papers on distinct sacking cases on Earth in which the sacking triggering mechanism has been explicitly discussed by the authors (Supplementary Table 1), 39 conclude that sacking is strictly a paraglacial process. According to these studies, slope debutting by the removal of valley glaciers on both sides of topographic ridges is a key process for sacking to initiate, and may be in some cases assisted by postglacial unloading and rebound (Jarman, 2006). Two other articles suggest that it is a paraglacial process assisted by regional neotectonic activity, two others ascribe sacking fault scarps to collateral events of intense seismic shaking on a nearby fault with no discussion about the possible influence of past glaciations, and one sacking case has an unidentified origin.

In the paraglacial environment, ridge debutting is mandatory, but not sufficient for sacking to initiate; otherwise sacking would pervasively affect many terrestrial mountain ranges, which is far from being the case. Factors promoting sacking have not been comprehensively investigated; nevertheless the following have been shown to be of primary importance, altogether or in partial combination. Wallslope height and glacial oversteepening (Beget, 1985) must first concur to bring the topography close to destabilisation. Chemical alteration by groundwater flow has been shown to actively participate to ridge decohesion, as illustrated by accumulations of clay minerals at the bottom of crestal graben scarps (Hippolyte et al., 2006). Ridge confinement by glacial load and subsequent debutting after valley deglaciation may also significantly decrease ridge rock mass strength (Cossart et al., 2008; Reitner and Linner, 2009) through mechanisms that have not been clearly identified but may include stress corrosion of

existing discontinuities and subcritical crack growth, and hydraulic fracturing in response to e.g. melting/freezing cycles. The orientation of the rock pre-existing discontinuities, such as stratification planes, faults, joints, and schistosity, may guide the geometry of the sacking features (Chigira, 1992; Nemčok, 1977; Nemčok and Baliak, 1977; Reitner and Linner, 2009; Ustaszewski et al., 2008) but are not required for sacking to operate. Selective weakening of lithologic sequences, for instance preferential alteration of horizontal volcanic tuff levels to argillite, produces mechanical contrasts that may assist in sacking initiation (Beget, 1985). Both the existence of major discontinuities and alternating lithological sequences pertain to the case of Valles Marineris, where the wallrock is dominantly a succession of subhorizontal volcanic layers of contrasting albedo (McEwen et al., 1999) of possibly different composition, that were probably fractured by thermal contraction following their emplacement and by regional tectonic extension and dyke emplacement during chasma initiation (Mège, 2001; Mège and Masson, 1996b).

#### 4. Further evidence of glaciation in Valles Marineris chasmata

From the excellent correlation between sacking occurrences and paraglacial settings on Earth, we infer that sacking in Valles Marineris is likely to result from deglaciation of the ridge-surrounding chasmata. This interpretation is supported by a series of morphological and mineralogical similarities between chasmata in Valles Marineris and formerly glaciated valleys on Earth.

Valles Marineris chasmata have steep walls where the bedrock displays spur-and-gully morphologies and flat floors where the bedrock is covered with soft sediments (Figs. 2b, 3, 4a,d, 5, 6). On Earth, these features are characteristic of formerly glaciated valleys

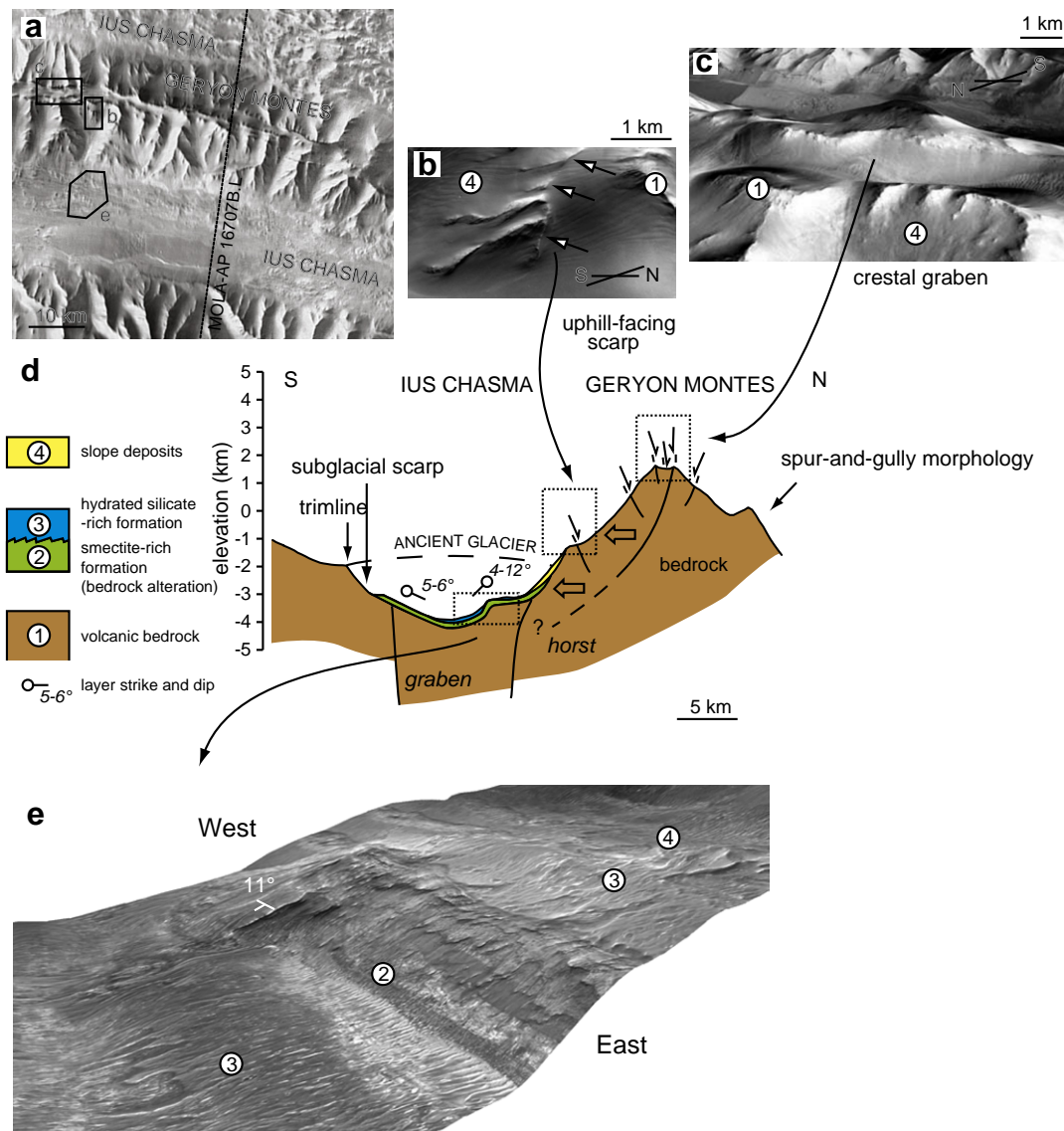


**Fig. 4.** Examples of sacking features in Ius Chasma and geological cross section along MOLA topographic profile MOLA-AP 16707B.L. Chasma floor deposits are identified following mineralogical interpretation from Roach et al. (2010), who also noted the erosional surface between the smectite-rich layers and the overlying hydrated silicate-rich formation. The three-dimensional views are THEMIS day-time images draped over HRSC DEM. Location in Fig. 1.

(Fig. 2a). Spur-and-gully morphology on walls of terrestrial glacial valleys is due to periglacial weathering processes acting above the surface of glaciers, whereas flat valley floors generally correspond to glacial and/or post-glacial sedimentary infills (Evans, 2005). As we shall now discuss, both walls and floors of Valles Marineris chasmata have morphological similarities with slopes and floors of terrestrial glacial valleys.

In areas of Valles Marineris where the spur-and-gully morphology has not been removed by further erosional processes, the base of the chasma walls usually displays a continuous scarp that is generally mantled by debris (Figs. 3, 4a, 5, 6, 8–10). Spurs and gullies are systematically located above this basal scarp. In an earlier work (Peulvast et al., 2001), we interpreted such basal scarps as normal fault scarps. However, (1) the continuous basal scarp described here runs nearly parallel to topographic contours, hence has a curvilinear shape in map view (Fig. 3), which is inconsistent with the rectilinear shape that would be expected for high-angle normal faults; (2) it does not display any evidence of the constant fault length/maximum displacement ratio that would be expected if it

was of tectonic origin, like e.g. the narrow grabens observed around Valles Marineris do (Schultz, 1997); (3) normal fault displacement profiles have tapered ends (e.g., Cowie and Scholz, 1992), which is not observed for the Valles Marineris continuous basal scarp discussed here; (4) terrestrial faults are segmented and commonly display en échelon patterns (Crider and Peacock, 2004; Mansfield and Cartwright, 2001; Olson and Pollard, 1991), which is not observed for the Valles Marineris basal continuous scarp either. Some of the chasma grabens do display segmentation, especially the Ius and Coprates chasmata, but this segmentation appears as broad-scale offsets in spur-and-gully alignments, not as offsets in alignments of individual basal scarps (Peulvast et al., 2001). Instead of fault scarps, we suggest that the best interpretation for this continuous basal scarp is subglacial erosion of the bedrock by valley glaciers that formerly covered the chasma floors. Nearly constant scarp height over long distances, independent of graben segmentation inferred from spur-and-gully patterns, and absence of scarp segmentation, are in agreement with this interpretation.

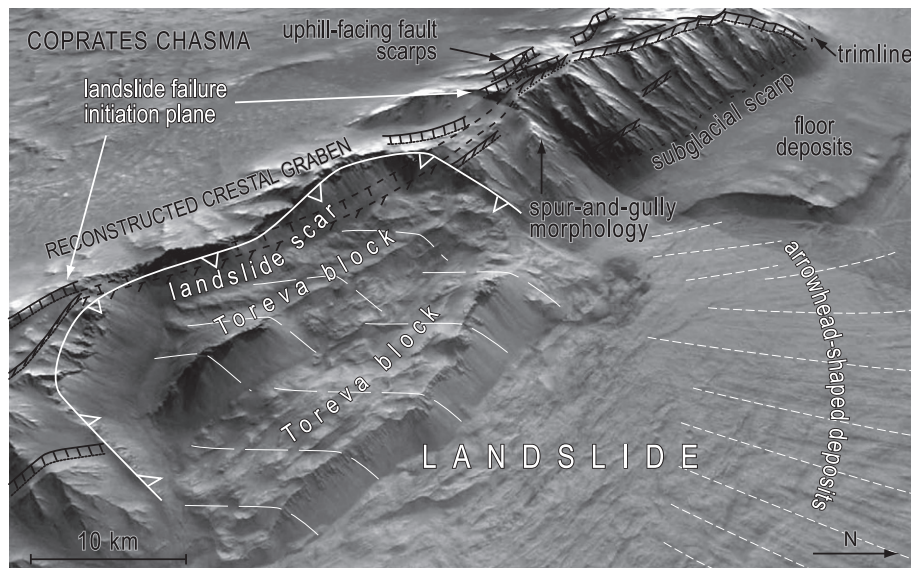


**Fig. 5.** Perspective view of the Coprates Chasma landslide. Sackung-related tectonic structures and glacial morphology are shown in black and landslide-related structures in white. The landslide scar is aligned with the uphill-facing normal fault scarps of the sackung crestral graben located on the slope opposite to landslide displacement. The arrowhead-shaped debris aprons indicate a steep landslide failure plane (Lucas et al., submitted), consistent with initiation from an existing normal fault. THEMIS image mosaic draped over HRSC digital elevation model. Location in Fig. 1.

The trimline marking the boundary between the subglacially eroded basal scarp and the overhanging periglacial spur-and-gully morphology can be identified in many parts of Valles Marineris (e.g. Figs. 3, 4a, 5, 6, 8–10) but it has frequently been eroded or covered by debris accumulations. Trimline height above chasma floor can be used to infer the maximal thickness of the former glacial infill; measured values in Ius and Candor chasmata (Fig. 9) are in the range of a few hundred metres to more than 1 km.

Many landforms on chasma floors can be interpreted as having a glacial origin also. Hummocky terrains, composed of roughly circular mounds and closed depressions, are observed at the base of some ridges affected by sackung (Figs. 9a,d and 10a,c,h,j). These terrains are similar in morphology to terrestrial hummocky ablation moraines deposited by vanishing glaciers (Fig. 10g,i; Gravenor and Kupsch, 1959; Evans, 2005, 2009). Associated to these hummocky terrains on some chasma floors, are groove-and-ridge terrains (Fig. 9a,b) that are similar in morphology to terrestrial streamlined moraines (Fig. 9c, Clark and Stokes, 2001; Evans, 2005). Dark deposits that partially cover these terrains (Figs. 9a–b and 10c) may have

accumulated more recently by, e.g., aeolian deposition. Alternatively, they might correspond to glacial ablation tills similar to those described in Noachis Terra (Fenton, 2005) and on the present-day North Polar Cap (Massé et al., 2010).

Two kinds of mineralogical observations also are consistent with the interpretation that glaciations and sackung occurred in Valles Marineris: (1) Wallrock-derived smectites have abundantly accumulated at the base of the Geryon Montes sackung area (Fig. 4d) (Roach et al., 2010). From comparison with terrestrial observations (e.g. Kobayashi, 1956) and laboratory modelling of expandable clay stability (Grygar et al., 2005), this suggests ridge weakening by chemical alteration in an abundance that makes a periglacial depositional environment likely; (2) Both sulphates and hydrated silica have been identified in sedimentary deposits covering chasma floors (Gendrin et al., 2005; Roach et al., 2010; Wendt et al., 2011). In other regions of Mars, these minerals have been convincingly interpreted as products of silicate material weathering in ancient ice deposits (Massé et al., 2010; Niles and Michalski, 2009).

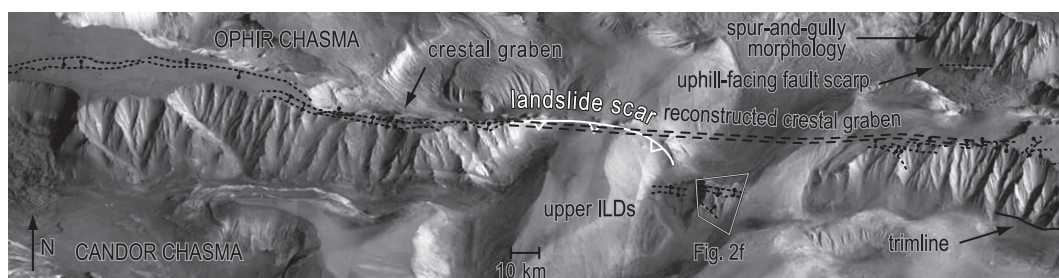


**Fig. 6.** Perspective view of the Candor–Ophir chasma boundary. The Candor–Ophir boundary is a horst in various stages of preservation that displays sackung structures. Sackung-related tectonic structures and glacial morphology are shown in black and landslide-related structures are in white. In areas where the plateau surface has been fully eroded the boundary is a ridge that displays a crestal graben with uphill-facing normal fault scarps. The circles point toward the downdip direction. Landsliding destroyed the crestal graben in the central area. The landslides and part of the initial, spur-and-gully wallslope morphology have been wholly covered by the upper unit of the Interior Layer Deposits (ILDs), of upper Hesperian–lower Amazonian age (Lucchitta, 1999). Part of vintage NASA/JPL mosaic PIA00005 obtained from Viking orbiter images.



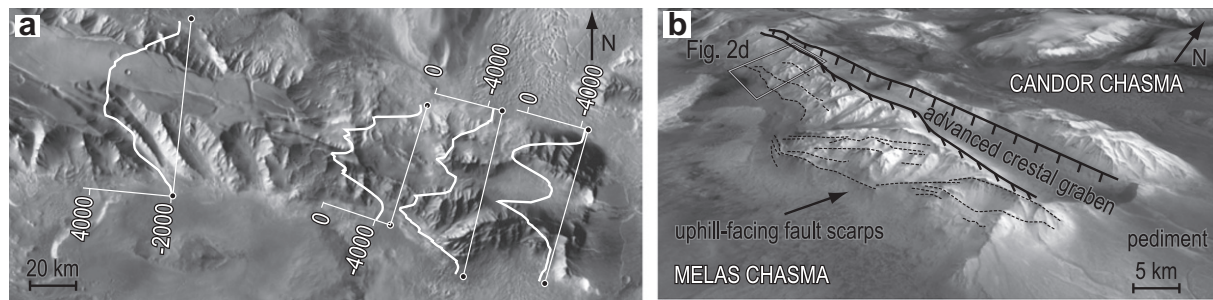


**Fig. 7.** Sackung at the Melas–Candor chasma boundary. a, THEMIS mosaic and topographic profiles after MOLA digital elevation model (elevation is in metres). The dots locate the profile ends. Note the gradual sinking of the inter-chasma plateau from west to east on the MOLA profiles. b, Plateau splitting is interpreted as the consequence of an eastward deepening central graben. THEMIS image mosaic draped over HRSC digital elevation model.

## 5. Timing

The younger limit for the sackung (and glaciation) age is given, at the Candor–Ophir boundary, by the upper Hesperian–lower Amazonian deposition age (Lucchitta, 1999) of the top of the ILDs, the deposition of which postdates post-sackung landsliding (Fig. 6). This minimum age is consistent with the interpretation of glacial events adjacent to Valles Marineris during the upper Hesperian, the possible jökulhlaups identified by Zealey (2009) in the Echus Chasma area. The maximum age is given in central Candor Chasma. The ILDs have been subdivided into two units of contrasting morphology and spectral characteristics (Le Deit et al., 2008); existence of a trimline along the lower ILDs on one northern side of central Candor Chasma and a trimline associated with sackung features on the southern side, indicate erosion by valley glacier after the deposition of the lower ILD sequence (Figs. 9 and 10).

## 6. Comparison with climate models

Observational evidence of past tropical and mid-latitude glaciations has been found on Mars (Head et al., 2005). Equatorial glaciations in Valles Marineris are specifically predicted by Mars General Circulation Models (GCMs) during periods of higher obliquity (Madeleine et al.,

2010), the existence of which has been demonstrated for the last 10 million years (Levrard et al., 2004). For older periods, obliquity variations are not well constrained but are likely to have been also variable.

Glaciations could have alternatively occurred while Valles Marineris was in a polar location. A magnetic paleopole has been proposed at Noctis Labyrinthus, at the western end of Valles Marineris (Arkani Hamed and Boutin, 2004). However, paleopole location can be inferred for the Noachian only due to subsequent dynamo switch-off.

The Hesperian to lower Amazonian glaciation of Valles Marineris described here occurred in a time span comprised between the recent past that is accessible with GCMs, and the ancient past while the core dynamo was still active. Its context and origin is therefore not well constrained, but GCMs and paleopole models do show that mechanisms exist that may help correlate Valles Marineris glaciations with global planetary processes.

## 7. Conclusions

The horsts that are observed in Valles Marineris have recorded a geological history that complements the list of events that have been identified in the chasmata, such as tectonic stretching in

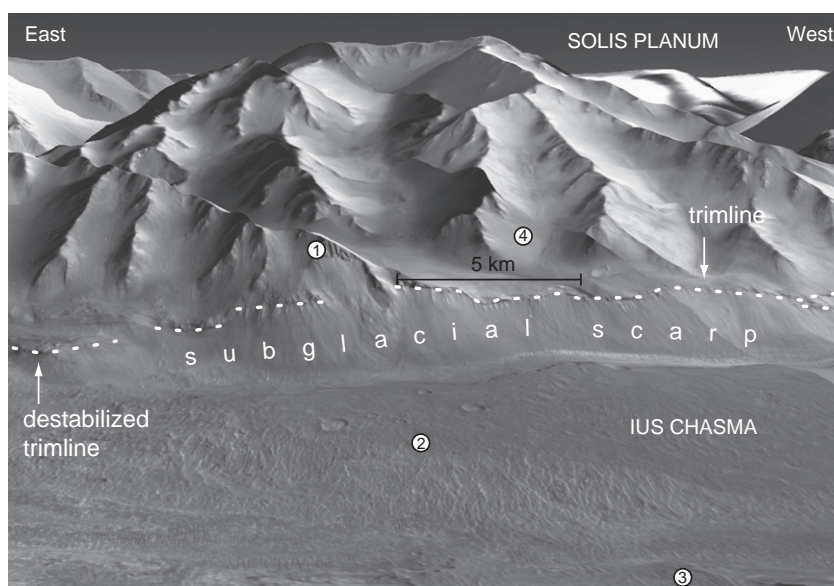


**Fig. 8.** Example of trimline and subglacial scarp in Valles Marineris: the southern Ius Chasma wallslope. The subglacial scarp is mantled by scree. HiRISE image ID# CTX\_P03\_002327\_1721 draped over HRSC digital elevation model. The numbers refer to the geological units identified in Fig. 4. Location in Fig. 1.

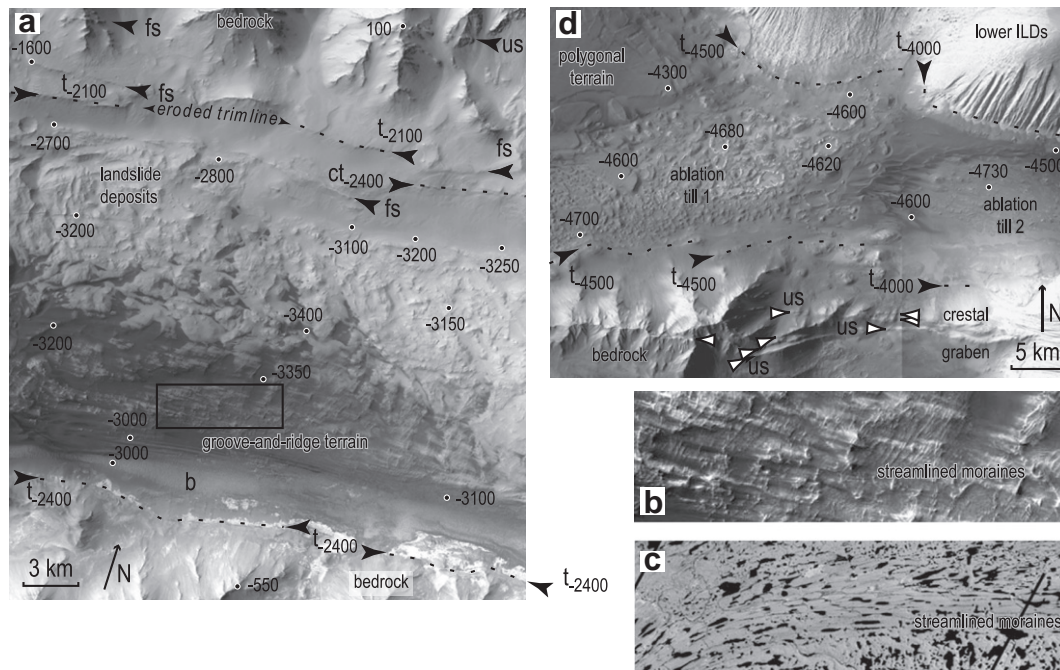


**Fig. 9.** a, Northern Ius Chasma graben showing scarps along the base of the chasma wall, interpreted to have a subglacial origin, and groove-and-ridge pattern on the floor parallel to the chasma wall. This pattern is interpreted as a streamlined glacial formation, partly blanketed by dark detrital materials. Part of CTX image P16\_007140\_1742. Location in Fig. 1. b, Zoom on the groove-and-ridge terrain. c, Streamlined moraines left by the M'Clintock Channel Ice Stream, Victorialand, Canadian Arctic (Clark and Stokes, 2001). The dark patches are postglacial lakes filling inter-morainic grooves. d, Hummocky terrain interpreted as ablation till in Central Candor Chasma, and surrounding wallslopes. The northern wallslope is a lower ILD mesa showing an erosional basal scarp interpreted as a subglacial scarp overlain by a trimline. The southern slope is a bedrock ridge also displaying a possible trimline as well as a crestal graben and uphill-facing scarps. In all the images, txxx: trimline, xxxx is the present approximate elevation in metres; ct: collapsed trimline; cm: controlled moraine; fs: fault scarp of undefined dip sense of dip angle; us: uphill-facing scarp; dots and associated numbers: mean HRSC elevation values at selected spots representative of geomorphologic units. These observations combined with observations in Fig. 6 suggest glaciations and paraglacial sacking after deposition of the lower ILDs and after deposition of the upper ILDs. Mosaic of CTX images P02\_001997\_1744 and P18\_007891\_1742 (location in Fig. 1). Fig. 10 gives a detailed interpretation of this mosaic and shows terrestrial analogues.

response to global dynamics, deposition of thick sequences of layered deposits, and large-scale landsliding. Geomorphologic and structural evidence points to a weakened ridge rheology after the main structural framework of Valles Marineris has been built, resulting in ridge sacking. Extensive examination of terrestrial analogues strongly suggests that ridge weakening results from valley deglaciation, an interpretation that is confirmed by geomorphological evidence of glaciated valleys in between the sagging horsts. Some of the sacking faults may be inherited from the early tectonic stretching history of Valles Marineris (Mège and Masson, 1996a; Mège et al., 2003; Peulvast et al., 2001; Schultz, 1991, 1995, 1998), similar to some sacking faults on Earth (e.g., Reitner and Linner, 2009).

The results presented here also imply the presence of a huge ice reservoir flowing in Valles Marineris in the past. The glaciations, of Hesperian to lower Amazonian age, i.e. between 3.5 Gy and 1.4 Gy (Hartmann and Neukum, 2001), provide clues to the Martian climate in a geological period for which constraints are still scarce. Their existence has implications for the origin and nature of the chaotic terrains

that are observed where Valles Marineris opens out, and the outflow channels that continue the chaotic terrains over 2000 km towards the northern lowlands.

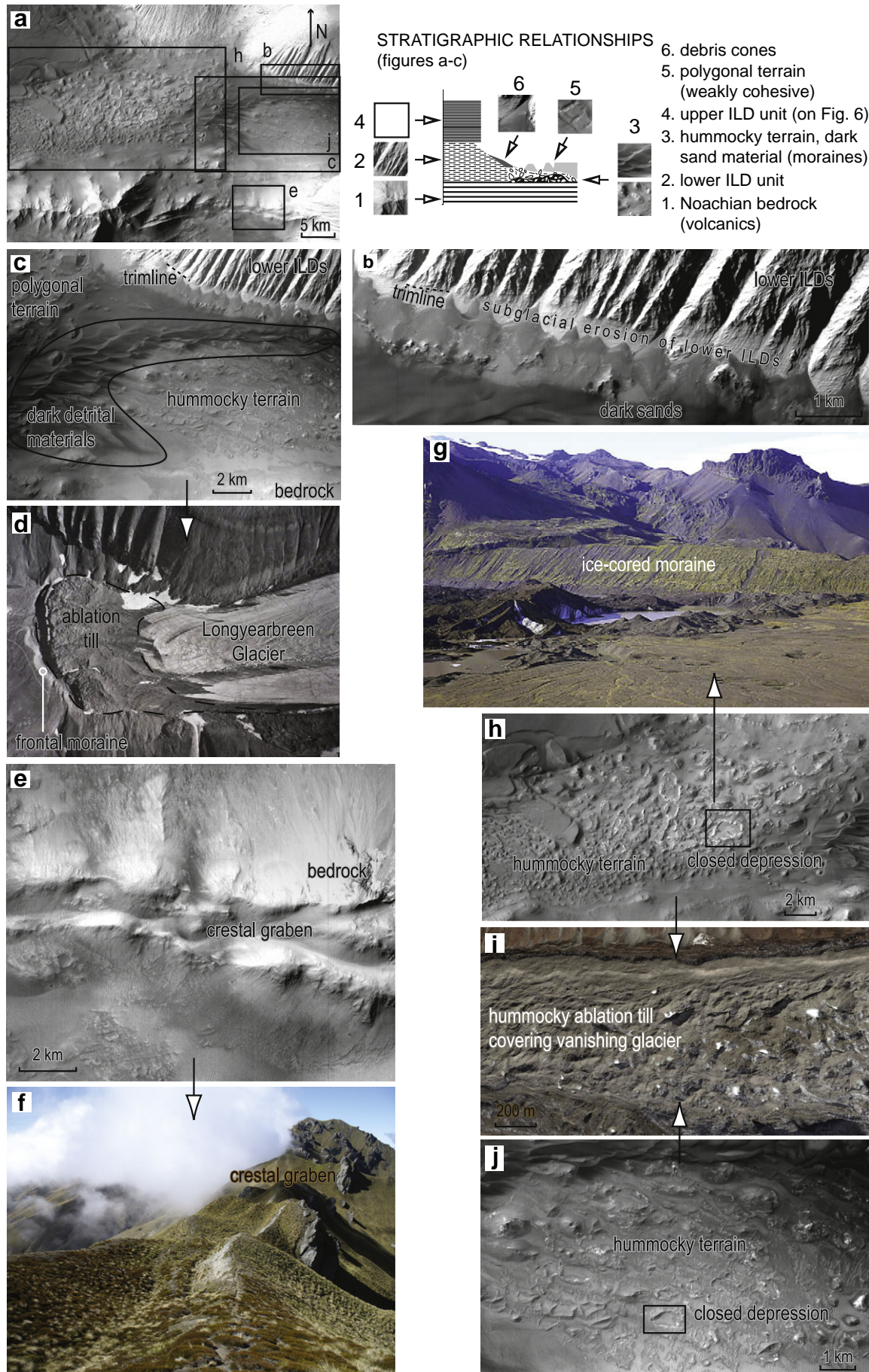
Supplementary data associated with this article can be found, in the online version, at [doi:10.1016/j.epsl.2011.08.030](https://doi.org/10.1016/j.epsl.2011.08.030).

### Acknowledgements

Credits for the data used in this study are: THEMIS, CTX: NASA/JPL/Arizona State University; HiRISE: NASA/JPL/University of Arizona; HRSC: ESA/DLR/FU Berlin; MOLA: NASA/JPL/GSFC. This work benefited from financial supports from the Centre National de la Recherche Scientifique, Institut National des Sciences de l'Univers (Programme National de Planétologie), from the Agence Nationale de la Recherche (Project ANR-08-JCJC-0126-MADMACS) and from the Centre National d'Etudes Spatiales. Comments by Chris Okubo and an anonymous referee led to clarification of several critical points in the manuscript.

**Fig. 10.** Glacial and paraglacial landforms in central Candor Chasma. a, Location map (same as Fig. 9d) and stratigraphic relationships in this area based on the following key relationships: (1) hummocky material, interpreted as ablation till, covers the lower ILD unit and is therefore more recent; (2) dark detrital materials covers hummocky material; (3) based on contrasting competence, hummocky material is interpreted to be distinct from polygonal material, which mantles all the other observed units and is therefore the most recent terrain. The main difference with the U.S.G.S. geologic map (Lucchitta, 1999) is that hummocky material and dark detrital materials are interpreted to be older than proposed on this map (units named Adu and Afh). This difference may be due to the implicit assumption made on the map by Lucchitta (1999) that landform age can be used as a proxy for rock age. b, Zoom on subglacial scarp and trimline affecting the base of a lower ILD unit. c–d, Comparison between the hummocky terrain and dark detrital materials in Candor Chasma (c) and loose morainic material in NW Ellesmere Island (Evans, 2009) that could be a dark detrital materials analogue. e–f, Crestal graben at the top of the sacking ridges: bedrock exposure located south of the hummocky material (e), and crest line between Alpha Peak and Roy's Peak near Wanaka, South Island, New Zealand (f, courtesy Colin Ballantyne). g–j, Ice-cored moraine left several decades ago by the Kvíárjökull Glacier in Iceland (Evans, 2009) (g), suggested analogues in Candor Chasma (h, j), and supraglacial moraine of an Himalayan glacier, northern Nepal (i, 30°8'30"N 82°8'E, Quickbird image), a suggested analogue of the Candor Chasma hummocky material.





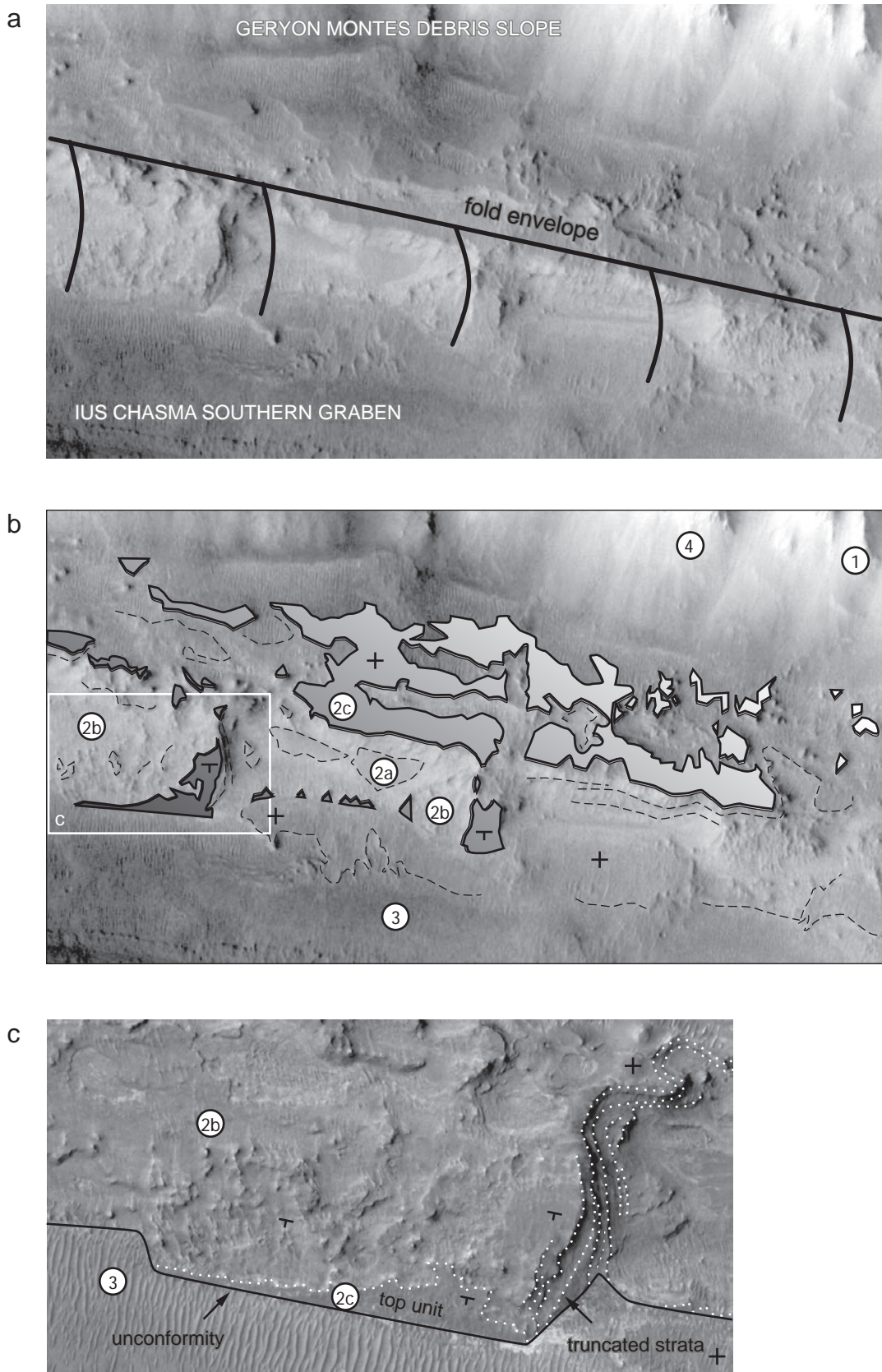


## References

- Arkani Hamed, J., Boutin, D., 2004. Paleomagnetic poles of Mars: revisited. *J. Geophys. Res.* 109. doi:10.1029/2003JE002229.
- Bachman, D., Bouissou, S., Chemenda, A., 2009. Analysis of massif fracturing during deep-seated gravitational slope deformation by physical and numerical modeling. *Geomorphology* 103, 130–135. doi:10.1016/j.geomorph.2007.09.018.
- Beget, J.E., 1985. Tephrochronology of antislope scarps on an alpine ridge near Glacier Peak, Washington, U.S.A. *Arctic Alpine Res.* 17, 143–152.
- Blasius, K.R., Cutts, J.A., Guest, J.E., Masursky, H., 1977. Geology of the Valles Marineris: first analysis of imaging from the Viking 1 Orbiter primary mission. *J. Geophys. Res.* 82, 4067–4091.
- Bos, B., Spiers, C.J., 2002. Fluid-assisted healing process in gouge-bearing faults: insights from experiments on a rock analogue system. *Pure Appl. Geophys.* 159, 2537–2566.
- Chigira, M., 1992. Long-term gravitational deformation of rocks by mass rock creep. *Eng. Geol.* 32, 157–184.
- Chojnacki, M., Hynek, B.M., 2008. Geological context of water-altered minerals in Valles Marineris, Mars. *J. Geophys. Res.* 113, E12005. doi:10.1029/2007JE003070.
- Clark, C., Stokes, C.R., 2001. Extent and basal characteristics of the McClinton Channel Ice Stream. *Quatern. Int.* 86, 81–101.
- Cossart, Braucher, R., Fort, M., Bourlès, D.L., Carcaillet, J., 2008. Slope instability in relation to glacial debuitressing in alpine areas (Upper Durance catchment, southeastern France): evidence from field data and  $^{10}\text{Be}$  cosmic ray exposure ages. *Geomorphology* 95, 3–26. doi:10.1016/j.geomorph.2006.12.022.
- Cowie, P., 1998. A healing–reloading feedback control on the growth rate of seismicogenic faults. *J. Struct. Geol.* 20, 1075–1087.
- Cowie, P.A., Scholz, C.H., 1992. Physical explanation for the displacement–length relationship of faults using a post-yield fracture mechanics model. *J. Struct. Geol.* 14, 1133–1148.
- Crider, J.G., Peacock, D.C.P., 2004. Initiation of brittle faults in the upper crust: a review of field observations. *J. Struct. Geol.* 26, 691–707.
- Disenza, M.E., Esposito, E., Martino, S., Petitta, M., Prestininzi, A., Scarascia Mugnozza, G., 2011. The gravitational slope deformation of Mt. Rocchetta ridge (central Apennines, Italy): geological–evolutionary model and numerical analysis. *Bull. Eng. Geol. Environ.* doi:10.1007/s10064-010-0342-7.
- Evans, D.J.A., 2005. *Glacial Landscapes*. Hodder Arnold, London. (532 pp.).
- Evans, D.J.A., 2009. Controlled moraines: origins, characteristics, and palaeogeological implications. *Quatern. Sci. Rev.* 28, 183–208. doi:10.1016/j.quascirev.2008.10.024.
- Fenton, L.K., 2005. Potential sand sources for the dune fields on Noachis Terra, Mars. *J. Geophys. Res.* 110, E11004. doi:10.1029/2005JE002436.
- Fuente, F., Stesky, R., McKinnon, P., Hauber, E., Zegers, T., Gwinn, K., Scholten, F., Neukum, G., 2008. Stratigraphy and structure of interior layered deposits in west Candor Chasma, Mars, from High Resolution Stereo Camera (HRSC) stereo imagery and derived elevations. *J. Geophys. Res.* 113, E10008. doi:10.1029/2007JE003053.
- Gendrin, A., Mangold, N., Bibring, J.-P., Langevin, Y., Gondet, B., Poulet, F., Bonello, G., Quantin, C., Mustard, J., Arvidson, R., Le Mouélis, S., 2005. Sulfates in Martian layered terrains: the Omega/Mars Express view. *Science* 307, 1587–1591.
- Gravenor, C.P., Kupsch, W.O., 1959. Ice-disintegration features in western Canada. *J. Geol.* 67 (1), 48–64.
- Grygar, T., Bezdička, P., Hradil, D., Hruskova, M., Novotna, K., Kadlec, J., Pruner, P., Oberhansli, H., 2005. Characterization of expandable clay minerals in Lake Baikal sediments by thermal dehydration and cation exchange. *Clays Clay Miner.* 53, 389–400.
- Guerricchio, A., Melidoro, G., 1979. Deformazioni gravitative profonde del tipo “sackung” nei monti di Maratea (Lucania). *Geol. Appl. Idrogeol.* 14, 13–22.
- Hartmann, W.K., Neukum, G., 2001. Cratering chronology and the evolution of Mars. *Space Sci. Rev.* 96, 165–194.
- Head, J.W., Neukum, G., Jaumann, R., Hiesinger, H., Hauber, E., Carr, M., Masson, P., Foing, B., Hoffmann, H., Kreslavsky, M., Werner, S., Milkovich, S., van Gasselt, S., the HRSC Co-Investigator Team, 2005. Tropical to mid-latitude snow and ice accumulation, flow and glaciation on Mars. *Nature* 434, 346–351.
- Hewitt, K., Clague, J.J., Orwin, J.F., 2008. Legacies of catastrophic rock slope failure in mountain landscapes. *Earth-Sci. Rev.* 87, 1–38.
- Hippolyte, J.-C., Brocard, G., Tardy, M., Nicoud, G., Bourlès, D., Braucher, R., Ménard, G., Souffaché, B., 2006. The recent fault scarps of the western Alps (France): tectonic surface ruptures or gravitational sackung scarps? A combined mapping, geomorphological, levelling, and  $^{10}\text{Be}$  dating approach. *Tectonophysics* 418, 255–276. doi:10.1016/j.tecto.2006.02.009.
- Hippolyte, J.-C., Bourlès, D., Braucher, R., Carcaillet, J., Léanni, L., Arnold, M., Aumaitre, G., 2009. Cosmogenic  $^{10}\text{Be}$  dating of a sackung and its faulted rock glaciers, in the Alps of Savoy (France). *Geomorphology* 108, 312–320. doi:10.1016/j.geomorph.2009.02.024.
- Jarman, D., 2006. Large rock slope failures in the Highlands of Scotland: characterisation, causes and spatial distribution. *Eng. Geol.* 83, 161–182. doi:10.1016/j.enggeo.2005.06.030.
- Kobayashi, K., 1956. Periglacial morphology of Japan. *Biuletyn Periglacialny* 4, 15–36.
- Le Deit, L., Le Mouélis, S., Combe, J.-P., Mège, D., Sotin, C., Gendrin, A., Hauber, E., Mangold, N., Bibring, J.-P., 2008. Ferric oxides in East Candor Chasma, Valles Marineris (Mars) inferred from analysis of OMEGA/Mars Express data: identification and geological interpretation. *J. Geophys. Res.* 113, E07001. doi:10.1029/2007JE002950.
- Levrard, B., Forget, F., Montmessin, F., Laskar, J., 2004. Recent ice-rich deposits formed at high latitudes on Mars by sublimation of unstable equatorial ice during low obliquity. *Nature* 431, 1072–1075.
- Lucas, A., Mangeney, A., Mège, D., and Bouchut, F. Scar geometry effect on landslide dynamics and deposit from granular modeling of Martian landslides. *J. Geophys. Res.*, in press.
- Lucchitta, B.K., 1977. Morphology of chasma walls, Mars. *J. Res. US Geol. Surv.* 6, 651–662.
- Lucchitta, B.K., 1981. Mars and Earth: comparison of cold-climate features. *Icarus* 45, 264–303.
- Lucchitta, B.K., 1999. Geologic map of Ophir and central Candor chasmata (MTM-05072) of Mars, U.S. Geol. Survey Atlas of Mars, 1:500,000 Geologic Series, map I-2568.
- Lucchitta, B.K., McEwen, A.S., Clow, G.D., Geissler, P.E., Singer, R.B., Schultz, R.A., Squyres, S.W., 1992. Valles Marineris. In: Kiefer, W.S., et al. (Ed.), *Mars*. Univ. Arizona Press, Tucson, pp. 453–492.
- Madeleine, J.-B., Forget, F., Head, J.W., Levrard, B., Montmessin, F., Millour, E., 2010. Amazonian northern mid-latitude glaciation on Mars: a proposed climate scenario. *Icarus* 203, 390–405. doi:10.1016/j.icarus.2009.04.037.
- Mahr, T., 1977. Deep-reaching gravitational deformations of high mountain slopes. *Bull. Int. Assoc. Eng. Geol.* 16, 121–127.
- Mansfield, C., Cartwright, J., 2001. Fault growth by linkage: observations and implications from analogue models. *J. Struct. Geol.* 23, 745–763.
- Marone, C., 1998. The effect of loading rate on static friction and the rate of fault healing during the earthquake cycle. *Nature* 391, 69–72.
- Massé, M., Bourgeois, O., Le Mouélis, S., Verpoorter, C., Le Deit, L., Bibring, J.-P., 2010. Martian polar and circum-polar sulfate-bearing deposits: sublimation tills derived from the North Polar cap. *Icarus* 209, 434–451.
- McEwen, A.S., Malin, M.C., Carr, M.H., Hartmann, W.K., 1999. Voluminous volcanism on early Mars revealed in Valles Marineris. *Nature* 397, 584–586.
- Mège, D., 2001. Uniformitarian plume tectonics: the post-Archean Earth and Mars. *Geol. Soc. Am. Spec. Pap.* 352, 141–164.
- Mège, D., Masson, P., 1996a. Amounts of crustal stretching in Valles Marineris, Mars. *Planet. Space Sci.* 44, 749–782.
- Mège, D., Masson, P., 1996b. A plume tectonics model for the Tharsis province, Mars. *Planet. Space Sci.* 44, 1499–1546.
- Mège, D., Cook, A.C., Lagabriele, Y., Garel, E., Cormier, M.-H., 2003. Volcanic rifting at Martian grabens. *J. Geophys. Res.* 108 (E5), 5044. doi:10.1029/2002JE001852.
- Nedell, S.S., 1987. Sedimentary geology of the Valles Marineris, Mars and Antarctic dry valleys lakes. NASA Tech. Memorandum, 89871, pp. 269–444.
- Nemčok, A., 1972. Gravitational slope deformation in high mountains. *Proc. 24th Int. Geol. Congr.*, 13, pp. 132–141.
- Nemčok, A., 1977. Geological/tectonical structures – an essential condition for genesis and evolution of slope movement. *Bull. Int. Assoc. Eng. Geol.* 16, 127–130.
- Nemčok, A., Baliak, F., 1977. Gravitational deformations in Mesozoic rocks of the Carpathian mountain ranges. *Bull. Int. Assoc. Eng. Geol.* 16, 109–111.
- Niles, P.B., Michalski, J., 2009. Meridiani Planum sediments on Mars formed through weathering in massive ice deposits. *Nat. Geosci.* 2, doi:10.1038/NGE0438.
- Okubo, C.H., 2010. Structural geology of Amazonian-aged layered sedimentary deposits in southwest Candor Chasma, Mars. *Icarus* 207, 210–225. doi:10.1016/j.icarus.2009.11.012.
- Okubo, C.H., Lewis, K.W., McEwen, A.S., Kirk, R.L., 2008. Relative age of interior layered deposits in southwest Candor Chasma based on high-resolution structural mapping. *J. Geophys. Res.* 113, E12002. doi:10.1029/2008JE003181.
- Olsen, M.P., Scholz, C.H., Léger, A., 1998. Healing and sealing of a simulated fault gouge under hydrothermal conditions: implications for fault healing. *J. Geophys. Res.* 103, 7421–7430.
- Olson, J.E., Pollard, D.D., 1991. The initiation and growth of en échelon veins. *J. Struct. Geol.* 13, 595–608.
- Peulvast, J.-P., Masson, P., 1993a. Melas Chasma: morphology and tectonic patterns in central Valles Marineris (Mars). *Earth Moon Planets* 61, 219–248.
- Peulvast, J.-P., Masson, P., 1993b. Erosion and tectonics in central Valles Marineris (Mars): a new morpho-structural model. *Earth Moon Planets* 61, 191–217.
- Peulvast, J.-P., Mège, D., Chiciak, J., Costard, F., Masson, P., 2001. Morphology, evolution, and tectonics of Valles Marineris wall slopes (Mars). *Geomorphology* 37, 329–352.
- Reitner, J.M., Linner, M., 2009. Formation and preservation of large scale toppling related to Alpine tectonic structures – Eastern Alps. *Aust. J. Earth Sci.* 102, 69–80.
- Reitner, J., Lang, M., van Husen, D., 1993. Deformation of high slopes in different rocks after Würmian deglaciation in the Gailtal (Austria). *Quatern. Int.* 18, 43–51.
- Roach, L.H., Mustard, J.F., Swayze, G., Milliken, R.E., Bishop, J.L., Murchie, S.L., Lichtenberg, K., 2010. Hydrated mineral stratigraphy in Ius Chasma, Valles Marineris. *Icarus* 206, 253–268. doi:10.1016/j.icarus.2009.09.003.
- Savage, W.Z., Varnes, D.J., 1987. Mechanics of gravitational spreading of steep-sided ridges (“sackung”). *Bull. Int. Assoc. Eng. Geol.* 35, 31–36.
- Schultz, R.A., 1991. Structural development of Coprates Chasma and western Ophir Planum, Valles Marineris rift, Mars. *J. Geophys. Res.* 96, 22,777–22,792.
- Schultz, R.A., 1995. Gradients in extension and strain at Valles Marineris, Mars. *Planet. Space Sci.* 43, 1561–1566.
- Schultz, R.A., 1997. Displacement–length scaling for terrestrial and Martian faults: implications for Valles Marineris and shallow planetary grabens. *J. Geophys. Res.* 102, 12,009–12,015.
- Schultz, R.A., 1998. Multiple-process origin of Valles Marineris basins and troughs, Mars. *Planet. Space Sci.* 46, 827–834.
- Sharp, R.P., 1973. Mars: troughed terrain. *J. Geophys. Res.* 78 (20), 4063–4072.
- Treiman, A., 2008. Ancient groundwater flow in the Valles Marineris on Mars inferred from fault trace ridges. *Nat. Geosci.* 1, 181–183. doi:10.1038/ngeo131.
- Ustaszewski, M., Hampel, A., Pfiffner, O.A., 2008. Composite faults in the Swiss Alps formed by the interplay of tectonics, gravitation and postglacial rebound: an integrated field and modelling study. *Swiss J. Geosci. (Eclogae Geologicae Helveticae)* 101, 223–235.
- Varnes, D.J., Radbruch-Hall, D.H., Savage, W.Z., 1989. Topographic and structural conditions in areas of gravitational spreading of ridges in the western United States. *U.S. Geol. Surv. Prof. Pap.*, 1496 (28 pp.).
- Wendt, L., Gross, C., Kneissl, T., Sowe, M., Combe, J.P., Le Deit, L., McGuire, P., Neukum, G., 2011. Sulfates and iron oxides in Ophir Chasma, Mars, based on OMEGA and CRISM observations. *Icarus* 213, 86–103.
- Zealey, W.J., 2009. Glacial, periglacial and glacio-volcanic structures on the Echus plateau, upper Kasei Valles. *Planet. Space Sci.* 57, 699–710.
- Zischinsky, U., 1966. On the deformation of high slopes. *Proc. 1st Congr. Int. Soc. Rock Mechanics*, 2, pp. 179–185.

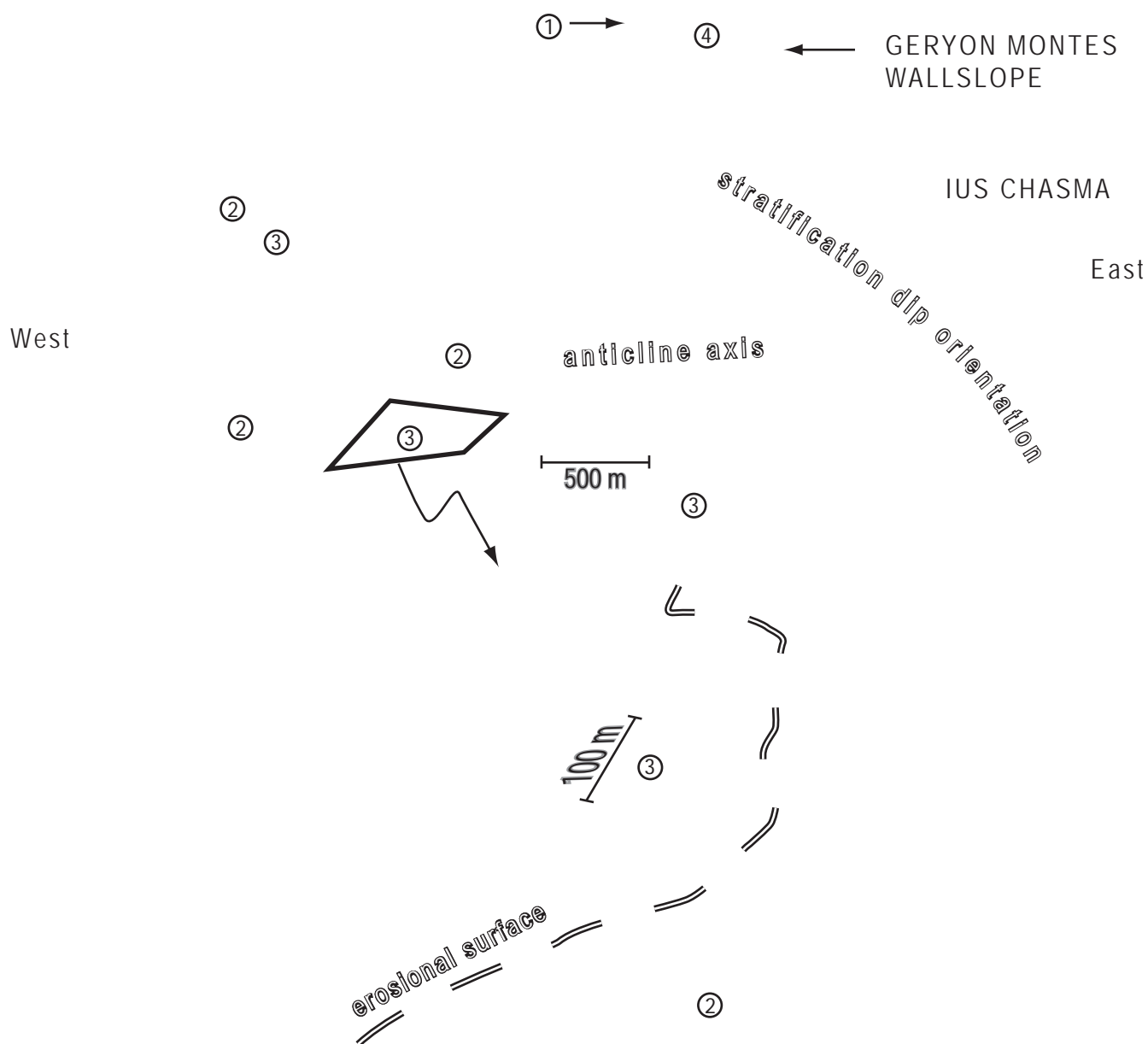
Main sackung trigger	Subsequent landsliding reported	Article
Regional seismicity (seismic slip on other fault)		<p><b>Ponti, D., and Wells, R.E., 1991.</b> Off-fault ground ruptures in the Santa Cruz Mountains, California: ridge-top spreading versus tectonic extension during the 1989 Loma Prieta earthquake. <i>Bull. Seism. Soc. Am.</i> 81, 1480-1510.</p> <p><b>Harp, E.L., and Jibson, R.W., 1996.</b> Landslides triggered by the 1994 Northridge, California, Earthquake. <i>Bull. Seismol. Soc. Am.</i> 86, S319-S332.</p>
Lateral debuttressing and/or Quaternary valley unloading after deglaciation in collisional orogens (either seismic or creep)		<p><b>Kobayashi, K., 1956.</b> Periglacial morphology of Japan. <i>Biuletyn Periglacjalny</i> 4, 15-36.</p> <p><b>Beck, A.C., 1968.</b> Gravity faulting as a mechanism of topographic adjustment. <i>New Zealand J. Geol. Geophys.</i> 11, 191–199.</p> <p><b>Tabor, R.W., 1971.</b> Origin of ridge-top depressions by large-scale creep in the Olumpic Mountains, Washington. <i>Geol. Soc. Am. Bull.</i> 82, 1811-1822.</p> <p><b>Radbrush-Hall, D.H., Varnes, D.J., and Savage, W.Z., 1976.</b> Gravitational spreading of steep-sided ridges ("sackungen") in western United States. <i>Int. Assoc. Eng. Geol. Bull.</i> 14, 28-35.</p> <p><b>Bovis, M.J., 1982.</b> Uphilll-facing (antislope) scarps in the Coast Mountains, southwest British Columbia. <i>Geol. Soc. Am. Bull.</i> 93, 804-812.</p> <p><b>Beget, J.E., 1985.</b> Tephrochronology of antislope scarps on an alpine ridge near Glacier Peak, Washington, U.S.A. <i>Arctic Alpine Res.</i> 17, 143-152.</p> <p><b>Holmes, G., and Jarvis, J.J., 1985.</b> Large-scale toppling with a sackung type deformation at Ben Attow, Scotland. <i>Q. J. Eng. Geol. London</i> 18, 287-289.</p> <p><b>Shroder, J.F., Jr., 1989.</b> Slope failure: Extent and economic significance in Afghanistan and Pakistan, in <i>Landslides: Extent and economic significance</i> (eds Brabb, E.E., and Harrod, B.L.) Balkema, 325-341.</p> <p><b>Varnes, D.J., Radbruch-Hall, D.H., and Savage, W.Z., 1989.</b> Topographic and structural conditions in areas of gravitational spreading of ridges in the western United States. <i>U.S. Geol. Surv. Professional Paper</i> 1496, 28 p.</p> <p><b>Varnes, D.J., Radbruch-Hall, D.H., Varnes, K.L., Smith W.K., and Savage, W.Z., 1990.</b> Measurement of ridge-spreading movements (Sackungen) at Bald Eagle Mountain, Lake County, Colorado, 1975-1989. <i>U.S. Geol. Surv. Open-File Rept.</i> 90-543, 15 p.</p> <p><b>Thorsen, G.W., 1989.</b> Splitting and sagging mountains. <i>Washington Geologic Newsletter</i> 17, 4, 3-13.</p> <p><b>Reitner, J., Lang, M., and van Husen, D., 1993.</b> Deformation of high slopes in different rocks after würmian deglaciation in the Gailtal (Austria). <i>Quaternary Int.</i> 18, 43-51.</p> <p><b>Bovis, M.J., and Evans, S.G., 1996.</b> Extensive deformations of rock slopes in southern Coast Mountains, southwest British Columbia, Canada. <i>Eng. Geol.</i> 44, 163-182.</p> <p><b>Ego, F., Sébrier, M., Carey-Gailhardis, E., and Beate, B., 1996.</b> Do the Billecocha normal faults (Ecuador) reveal extension due to lithospheric body forces in the northern Andes? <i>Tectonophysics</i> 265, 255-273.</p> <p><b>Bovis, M.J., and Jakob, M., 2000.</b> The July 29, 1998, debris flow and landslide dam at Capricorn Creek, Mont Meager Volcanic Complex, southern Coast Mountains, British Columbia. <i>Can. J. Earth Sci.</i> 37, 1321-1334.</p> <p><b>Varnes, D.J., Coe, J.A., Godt, J.W., Savage, W.Z., and Savage, J.E., 2000.</b> Measurement of ridge-spreading movements (sackungen) at Bald Eagle Mountain, Lake County, Colorado, II: continuation of the 1975-1989 measurements using a Global Positioning System in 1997 and 1999. <i>U.S. Geol. Survey Open-File Rept.</i> 00-205, 23 p.</p> <p><b>Agliardi, F., Crosta, G., and Zanchi., A., 2001.</b> Structural constraints on deep-seated slope deformation kinematics. <i>Eng. Geol.</i> 59, 83-102 (2001).</p> <ul style="list-style-type: none"> <li><b>Smith, L.N., 2001.</b> Columbia Mountain landslide: late-glacial emplacement and indications of future failure, Northwestern Montana, U.S.A. <i>Geomorphology</i> 41, 309-322.</li> </ul> <p><b>Jarman, D., and Ballantyne, C.K., 2002.</b> Beinn Fhada, Kintal: An example of large-scale paraglacial rock slope deformation. <i>Scottish Geog. J.</i> 118, 159-168.</p> <p><b>Hermann, S.W., and Becker, L.P., 2003.</b> Gravitational spreading ridges on the crystalline basement of the Eastern Alps (Niedere Tauern mountain range, Austria). <i>Mitt.Österr. Geol. Ges.</i> 94, 123-138.</p> <p><b>Holm, K., Bovis, M., and Jakob, M., 2004.</b> The landslide response of alpine basins to post-Little Ice Age glacial thinning and retreat in southwestern British Columbia. <i>Geomorphology</i> 57, 201-216.</p> <p><b>Kellog, K.S., 2004.</b> Thrust-induced collapse of mountains—An example from the "Big Bend" region of the San Andreas fault, western Transverse Ranges, California. <i>U.S. Geol. Surv. Sci. Invest. Rept.</i> 2004-5206, 10 p.</p> <p><b>Brückl, E., and Paroditis, M., 2005.</b> Prediction of slope instabilities due to deep-seated gravitational creep. <i>Natural Hazards Earth System Sci.</i> 5, 155-172.</p> <p><b>Hetzel, R., and Hampel, A., 2005.</b> Slip rate variations on normal faults during glacial-interglacial changes in surface loads. <i>Nature</i> 435, 81-84.</p> <p><b>Kinakin, D., and Stead, D., 2005.</b> Analysis of the distributions of stress in natural ridge forms: implications for the deformation mechanisms of rock slopes and the formation of sackung. <i>Geomorphology</i> 65, 85-100, doi:10.1016/j.geomorph.2004.08.002.</p> <ul style="list-style-type: none"> <li><b>Korup, O. ,2005.</b> Geomorphic imprint of landslides on alpine river systems, southwest New Zealand. <i>Earth Surf. Process. Landforms</i> 30, 783-800.</li> </ul> <p><b>Wilson, P., 2005.</b> Paraglacial rock-slope failures in Wasdale, western Lake District, England: morphology, styles and significance. <i>Proc. Geol. Assoc.</i> 116, 349-361.</p> <p><b>Ambrosi, C., and Crosta, G.B., 2006.</b> Large sackung along major tectonic features in the Central Italian Alps. <i>Eng. Geol.</i> 83, 183-200.</p> <p><b>Hippolyte, J.-C., Brocard, G., Tardy, M., Nicoud, G., Bourlès, D., Braucher, R., Ménard, G., and Souffaché, B., 2006.</b> The recent fault scarps of the western Alps (France): tectonic surface ruptures or gravitational sackung scarps? A combined mapping, geomorphic, levelling, and <sup>10</sup>Be dating approach. <i>Tectonophysics</i> 418, 255-276, doi:10.1016/j.tecto.2006.02.009.</p> <p><b>Hippolyte, J.-C., Tardy, M., and Nicould, G., 2006.</b> Les failles récentes des Grands-Moulins (Savoie) : un sackung (tassement gravitaire) majeur dans les Alpes françaises. <i>C. R. Geosci.</i> 338, 734-741.</p> <p><b>Hürlimann, M., Ledesma, A., Corominas, J., and Prat, P.C., 2006.</b> The deep-seated slope deformation at Encampadana, Andorra: representation of morphologic features by numerical modelling. <i>Eng. Geol.</i> 83, 343-357.</p> <p><b>Jarman, D., 2006.</b> Large rock slope failures in the Highlands of Scotland: Characterization, causes and spatial distribution. <i>Engineering Geol.</i> 83, 161-182.</p> <p><b>Turnbull, J.M., and Davies, T.R.H., 2006.</b> A mass movement origin for cirques. <i>Earth Surf. Process. Landforms</i> 31, 1129-1148.</p> <p><b>Wilson, P., and Smith, A., 2006.</b> Gomorphological characteristics and significance of Lat Quaternary paraglacial rock-slope failures on Skiddaw Group terrain, Lake District, northwest England. <i>Geografiska Annaler</i> 88, 237-252.</p> <p><b>Ustaszewski, M., Hampel, A., and Pfiffner, O.A., 2008.</b> Composite faults in the Swiss Alps formed by the interplay of tectonics, gravitation and postglacial rebound: an integrated field and modelling study. <i>Swiss. J. Geosci.</i> (Eclogae Geologicae Helvetiae) 101, 223-235.</p> <ul style="list-style-type: none"> <li><b>Hewitt, K., 2009.</b> Glacially conditioned rock-slope failures and disturbance-regime landscapes, upper Indus basin, northern Pakistan, in <i>Periglacial and Paraglacial Processes and Environments</i> (eds Knight, J., and Harrison, S.) <i>Geol. Soc. London, Sp. Publ.</i> 320, 235-255.</li> </ul> <p><b>Hippolyte, J.-C., Bourlès, D., Braucher, R., Carcaillet, J., Léanni, L., Arnold, M., and Aumaitre, G., 2009.</b> Cosmogenic <sup>10</sup>Be dating of a sackung and its faulted rock glaciers, in the Alps of Savoy (France). <i>Geomorphology</i> 108, 312-320.</p> <ul style="list-style-type: none"> <li><b>Jarman, D., 2009.</b> Paraglacial rock slope failure as an agent of glacial trough widening, in <i>Periglacial and Paraglacial Processes and Environments</i> (eds Knight, J., and Harrison, S.) <i>Geol. Soc. London, Sp. Publ.</i> 320, 103-131.</li> </ul> <p><b>Reitner, J., and Linner, M., 2009.</b> Formation and preservation of large scale toppling related to alpine tectonic structures – eastern Alps. <i>Austrian J. Earth Sci.</i> 102, 69-80.</p>
Paraglacial+active tectonics		<p><b>Jarman, D., 2002.</b> Rock slope failure and landscape evolution in the Caledonian mountains, as exemplified in the Abisko area, northern Sweden. <i>Geog. Annal.</i> 84A, 213-224.</p> <p><b>Audemard, F.A., Beck, C., and Carrillo, E., 2010.</b> Deep-seated gravitational slope deformations along the active Boconó Fault in the central portion of the Mérida Andes, western Venezuela. <i>Geomorphology</i> 124, 164-177, doi: 10.1016/j.geomorph.2010.04.020.</p> <ul style="list-style-type: none"> <li><b>Li, Z., Bruhn, R.L., Pavlis, T.L., Vorkink, L., and Zeng, Z., 2010.</b> Origin of sackung uphill-facing scarps in the Saint Elias orogen, Alaska: LIDAR data visualization and stress modeling. <i>Geol. Soc. Am. Bull.</i> 122, 1585-1599, doi:10.1130/B30019.1</li> </ul>
Unidentified (seismic shaking and rainfall dismissed)		<p><b>Rizzo, V., and Leggeri M., 2004.</b> Slope instability and sagging reactivation at Maratea (Potenza, Basilicata, Italy) <i>Eng. Geol.</i> 71, 181-198.</p>

Supplementary Table 1: Structured list of peer-reviewed publications on ridges affected by sackung in which favourable or triggering mechanisms have been explicitly discussed by the authors based on case studies. For ridges studied in more than one paper by the same authors, only one publication is mentioned.



Supplemental Figure 1. Floor deformation in Ius Chasma south of Geryon Montes. The numbers refer to the geological units identified on Fig. 4. Formation #2 has been divided in lower, middle, and upper units named 2a, 2b, and 2c respectively. HiRISE image ID# PSP 6863\_1720. Location on Fig. 3.





Supplemental Figure 2. Floor deformation in Ius Chasma south of Geryon Montes, east of Supplemental Figure 1, and stratigraphic relationships between formations #2 and #3. View is toward north. The unconformity between formations 2 and 3 has also been noted by Roach et al. (2010). The numbers refer to the geological formations identified on Figure 4. HiRISE image ID# PSP\_6863\_1720 draped over HRSC digital elevation model. Location on Fig. 3.